iScience

CellPress
OPEN ACCESS

Article

Flexible and excellent electromagnetic interference shielding film with porous alternating PVA-derived carbon and graphene layers

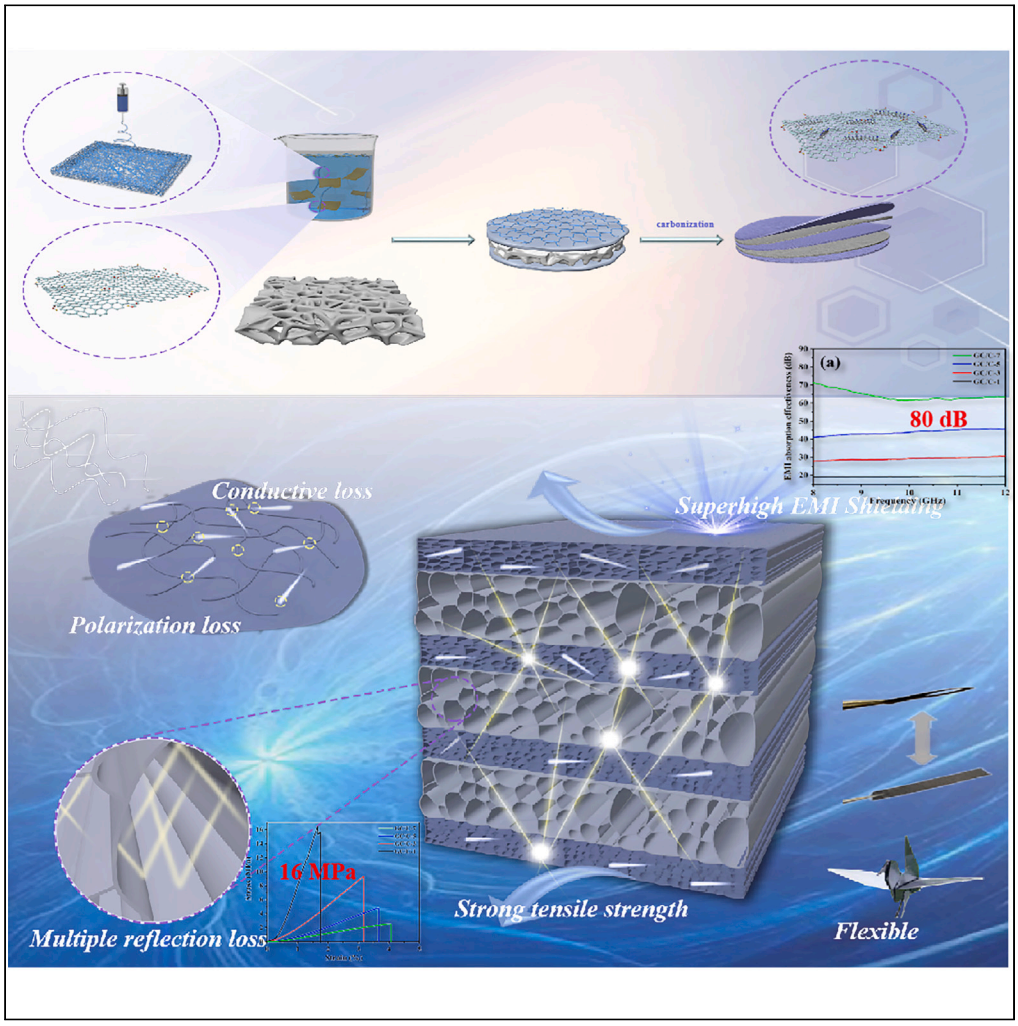

Jiatong Li, Jinzhe Li, Tian Li, ..., Qing Qi, Benliang Liang, Fanbin Meng

qi_qing7@163.com (Q.Q.)
blliang@bjtu.edu.cn (B.L.)
mengfanbin_wing@126.com (F.M.)

Highlights

The alternating film with 160 μm achieved an EMI SE of up to 80 dB in the X-band

Finite element analysis was applied to study the absorption mechanism of EM wave

The shielding properties of the film remained stable after 250 cycles

Li et al., iScience 26, 107975
October 20, 2023
https://doi.org/10.1016/j.isci.2023.107975

iScience

CellPress
OPEN ACCESS

Article

Flexible and excellent electromagnetic interference shielding film with porous alternating PVA-derived carbon and graphene layers

Jiatong Li,[1] Jinzhe Li,[1] Tian Li,[1] Zhengkang Xu,[1] Yao Chen,[1] Likui Zhang,[1] Qing Qi,[1,*] Benliang Liang,[3,*] and Fanbin Meng[1,2,4,*]

SUMMARY

Recently, the design of graphene-based films with elaborately controlled microstructures and optimized electromagnetic interference shielding (EMI) properties can effectively improve EM energy attenuation and conversion. Herein, inspired by the structure of multi-layer steamed bread, an alternating multilayered structure with polyvinyl alcohol (PVA)-derived carbon layers and graphene/electrospun carbon nanofibers layers was designed through alternating vacuum-assisted filtration method. The composite film exhibited favorable impedance matching, abundant loss mechanism, and excellent EMI shielding ability, resulting in absorption dominated shielding characteristic. Thus, the resultant 7-layer alternating composite films with a thickness of 160 μm achieved an EMI shielding effectiveness (EMI SE) of up to 80 dB in the X-band. Specially, finite element analysis was applied to demonstrate the importance of seven-layer film alternations and detailed analysis of electromagnetic shielding mechanisms. Taken together, this effort opens a creative avenue for designing and constructing flexible composite films with excellent EMI shielding performance.

INTRODUCTION

Electromagnetic radiation pollution has become a serious problem in today's society because of the rapid increase of the application of modern electronic components.[1–4] Therefore, how to suppress electromagnetic interference has become an important topic in the field of material development. Recently, in order to eliminate equipment damage,[5] health hazards[6,7] and other problems caused by electromagnetic wave pollution, preparing high efficiency electromagnetic protection materials by designing the microscopic or macroscopic structure of carbon-based materials has become a research hot topic.[8–11] There are two main ways of electromagnetic shielding. One way is to reflect electromagnetic waves so that they cannot enter the protected material, which requires a mismatch between the shielding layer and the air impedance, which is achieved through high conductivity. This method is usually used for dense, corrosion-prone metals, such as aluminum, copper, etc., which is difficult to be used for a long time in harsh environment, and the high quality increases the difficulty of use. The other way is to absorb the incident electromagnetic wave, which has a wider selection range of materials to avoid the defects of large weight, poor toughness and easy corrosion of metal materials, and also easier to carry out structural design, which can realize the loss effect of electromagnetic wave under a specific structure, so there are fewer restrictions on materials and more application prospects.[4] Due to the limitation of metal shielding materials and poor tunability, electromagnetic shielding film material which achieves the main shielding effect by absorption is still the main strategy for the preparation of EMI shield materials at present.[12–14] For example, Li[15] et al. developed the flexible, multi-field response MXene-Based Janus films with attractive EMI shielding effectiveness of 40 dB. Zhang[16] et al. prepared an alkali-treated polyacrylonitrile (aPAN) nanofibers reinforced graphene oxide (GO) composite film which shows excellent electromagnetic shielding effectiveness (SE) of 55~57 dB and the corresponding value of the specific SE/thickness can reach 70 dB cm^2/g. However, there is still a problem in the design and preparation of high efficiency shielding film materials that electromagnetic shielding properties and mechanical properties cannot be well coordinated, so it is urgent to develop the film with high mechanical strength and excellent EMI shielding properties.[17–19]

Graphene, the first two-dimensional material to become a cornerstone of materials science research since its discovery in 2004,[20,21] which has excellent mechanical strength, chemical stability and high conductivity, has broad application prospect in EMI shielding and microwave absorption (MA) field.[22–24] However, the problems of easy aggregation and high resistance of graphene sheets seriously affect the shielding effect, so it is necessary to design its structure. Meng[25] et al. designed an RGO-based film with "brick-slurry" structure which is conductive to

[1]Key Laboratory of Advanced Technologies of Materials (Ministry of Education), School of Materials Science and Engineering, Southwest Jiaotong University, Chengdu 610031, P.R. China
[2]Shenzhen Institute of Southwest Jiaotong University, Shenzhen 518000, China
[3]School of Physical Science and Engineering, Beijing Jiaotong University, Beijing 100044, China
[4]Lead contact
*Correspondence: qi_qing7@163.com (Q.Q.), blliang@bjtu.edu.cn (B.L.), mengfanbin_wing@126.com (F.M.)
https://doi.org/10.1016/j.isci.2023.107975

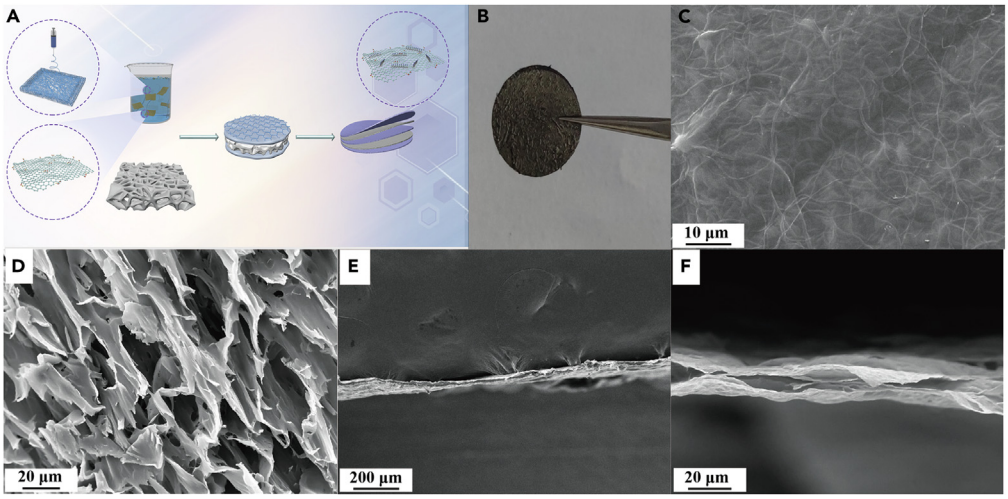

Figure 1. Preparation process and morphology control of GC/C-n films

(A–F) (A) Flow chart of preparation of GC/C films; (B) Optical photo of GC/C-7; (C) The surface morphology of GO/aPAN-PVA-7; (D) Morphological characterization of PVA aerogel; (E) Morphological characterization of GO/aPAN-PVA-1; (F) Morphological characterization of GC/C-1.

the construction of conductive path and shows great EMI performance, high strength, and excellent environmental adaptability. Zhang[26] et al. prepared $Ti_3C_2T_x$/rGO porous EMI shielding composite films by ion-induced self-assembly and vacuum-assisted filtration, which has high electrical conductivity and high EMI SE because it is dense in surface and porous inside. Liang[27] et al. designed a flexible polyvinylidene fluoride (PVDF) film with various heterogeneous alternating multilayer structures, which shows outstanding EMI performance and high thermal conductivity. Therefore, structural design such as porous design[28,29] or multilayer design[27,30–33] is often used to obtain graphene-based films with high shielding properties because it solves the problem of agglomeration between graphene sheets but also proficial to realize the increase of conductive paths, which can enhance the conductivity of the material and achieve high EMI shielding performance. Porous lightweight graphene EMI material has important application value in many fields while it remains a challenge to achieve efficient and controlled preparation of macroscopic three-dimensional porous graphene films.

In this work, inspired by the structure of multi-layer steamed bread, an excellent EMI shielding film with porous alternating PVA-derived carbon and graphene layers was prepared by a feasible alternating vacuum-assisted filtration method to combine the advantages of both structures, which achieved an EMI SE of up to 80 dB in the X-band with a thickness of 160 μm. The multi-layer structure inspired by the multi-layer steamed bread is designed in order to combine the advantages of the two structures, which can shield more electromagnetic waves while having excellent mechanical strength. What's more, the porous carbon alternating film shows the advantages of tunable thickness, high conductivity and great mechanical strength because of its multi-scale pore alternating structure, which comes from the multiple reflections of the porous structure, multilayer structure and the high conductivity of the film. Specially, the electromagnetic simulation was accomplished by using the finite element method (FEM) to prove that the alternating multilayer structure can effectively increase the loss of its internal electromagnetic wave, which improves its EMI SE. In addition, the tensile strength of up to 16 MPa and the stable conductivity and mechanical properties after 250 cycles of bending tests demonstrate the possibility of future applications in flexible electronic devices. This work can provide the prospect of long-term effective application in flexible equipment and an idea for novel structure design of graphene-based thin films, which will be beneficial to obtain an ultra-thin flexible electromagnetic protective film with mechanical stability and stable electromagnetic shielding performance.

RESULTS

Porous alternate polyvinyl alcohol-derived carbon and graphene-layered film (GC/C) was successfully synthesized through the scrape coating on PVA aerogel film by GO/aPAN solution (Figure 1A). The optical image (Figure 1B) shows that the surface of the film prepared is pleated, compared with the compact laminated graphene film, the GC/C film has a carbon porous structure and more interfaces, which is conducive to the multiple reflection loss and electromagnetic wave absorption, thus greatly improving the overall shielding performance of the film. Obviously, as the number of alternating layers increases, the thickness of the film also shows an increasing trend (3–160 μm). SEM images are exhibited from Figures 1C–1F and 2A–2G, which shows the morphologies and microstructures of GO/aPAN-PVA-n alternate film and GC/C-n alternating reduction film. The aPAN nanofibers are uniformly distributed on the GO surface, which is proved by Figure 1C, indicating that alkaline treatment and ultrasonic dispersion can disperse the intertangled long-size nanofibers and disperse uniformly in GO solution, which will be beneficial to the construction of conductive networks after high-temperature reduction treatment. As shown in Figure 1D, the PVA aerogel prepared by freeze-drying presents a relatively regular three-dimensional porous structure, which will be effective to the construction of porous structures in alternating films. The interfacial interaction between PVA and GO/aPAN forms the anchor structure through hydrogen

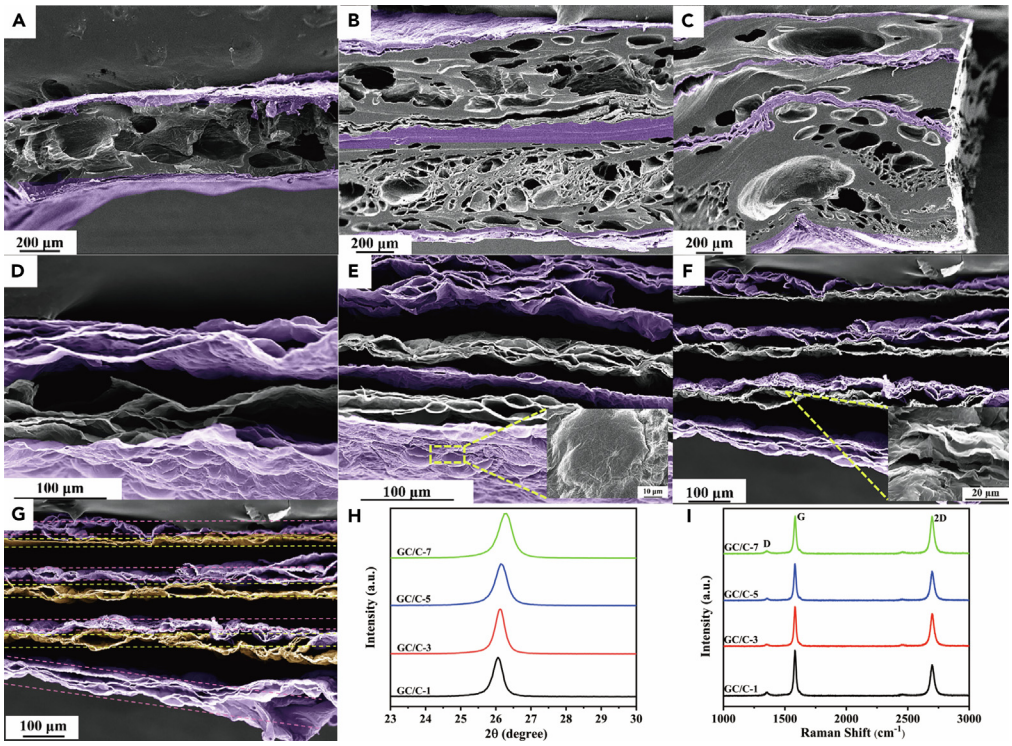

Figure 2. Morphology and structural characterization of GO/aPAN-PVA-n and GC/C-n film

(A–I) Morphological characterization of (A) GO/aPAN-PVA-3; (B) GO/aPAN-PVA-5; (C) GO/aPAN-PVA-7; (D) GC/C-3; (E) GC/C-5; (F) GC/C-7; (E) Surface microballoon structure of GC/C-5; (F) Interlayer structure of GC/C-7; (G) Layer thickness of GC/C-7; (H) XRD spectra of GC/C-n; (I) Raman spectra of GC/C-n.

bonding, which promotes the interfacial bonding and improves the interfacial strength. Comparing with the SEM of GO/aPAN-PVA-n (Figure 2A–2C), single-layer GO/aPAN thin film (GO/aPAN-PVA-1) has a dense structure as shown in Figure 1E, which indicates that the intermediate layer of the thin film prepared by alternating PVA presents a porous structure, and the thickness of the thin film increases with the increase of the number of layers. In particular, the interface between GO/aPAN and PVA could be clearly distinguished, indicating that the GO/aPAN-PVA-n alternating films were successfully prepared. Based on the aforementioned studies, GO/aPAN-PVA-n films were preoxidized at 200°C to improve the structural stability of aPAN nanofibers at high temperature, and then annealed at 1900°C to prepare porous graphene alternate films (GC/C-n). Their microstructure is shown by SEM (Figures 2A–2G), which exhibites that after pre-oxidation and high-temperature annealing reduction, carbon nanofiber-reinforced graphene film (GC/C-1) (Figure 1F) presents a loose layered structure, which is completely different from GO/aPAN film, mainly caused by the gases released by GO and aPAN during the defect repair process of graphene and carbon nanofibers, specially, this structure can improve the shielding effect of electromagnetic wave by increasing the number of reflections to a large extent.[35,36] Moreover, with the introduction of PVA, the above multilayer structure becomes more obvious (Figures 2D–2F), and the interlayer pore structure and thickness of the film are also increasing, which is mainly caused by the small gas molecules generated by the decomposition of PVA, GO, and PAN during the high-temperature annealing process. As can be seen from Figure 2E, in addition to the clearly visible microballoon structure that can be observed in the surface topography of GC/C-5 films (lower right corner of the figure), there are conductive networks formed by carbon nanofibers on the surface. The continuous conductive path required for the movement of free electrons can be provided by the mutual lap between the fibers to promote the increase of conductivity and facilitate the efficient shielding of the film. The morphology at the interface was characterized by SEM (Figure 2F) in order to further explore the connection state at the interface. As shown in the lower right corner of Figure 2F, the messy porous morphology is displayed at the interface of PVA after carbonization, which has a completely different structure from graphene, since there are obviously porous layer and dense layer after high temperature carbonization and a certain connection between them, when electromagnetic wave enters the structure, it can not only conduct well but also have polarization effect at the interface, and carry out multiple reflection loss in the hole, which can synergically enhance the EMI shielding effect.

In order to further explore whether GC/C films were successfully prepared and their crystal structure, XRD and Raman characterization were used, as shown in Figures 2H and 2I. The diffraction peaks of graphene-based films were observed to be narrow and sharp at about 26.1°(Figure 2H), indicating that the high temperature annealing treatment reduces the defects of the film structure, which represent that the graphene layers accumulate more regularly and have a more regular order after high temperature annealing. With the introduction of PVA and the increase of interlayer number, 2θ values showed an increasing trend, indicating that the alternating structure was conducive

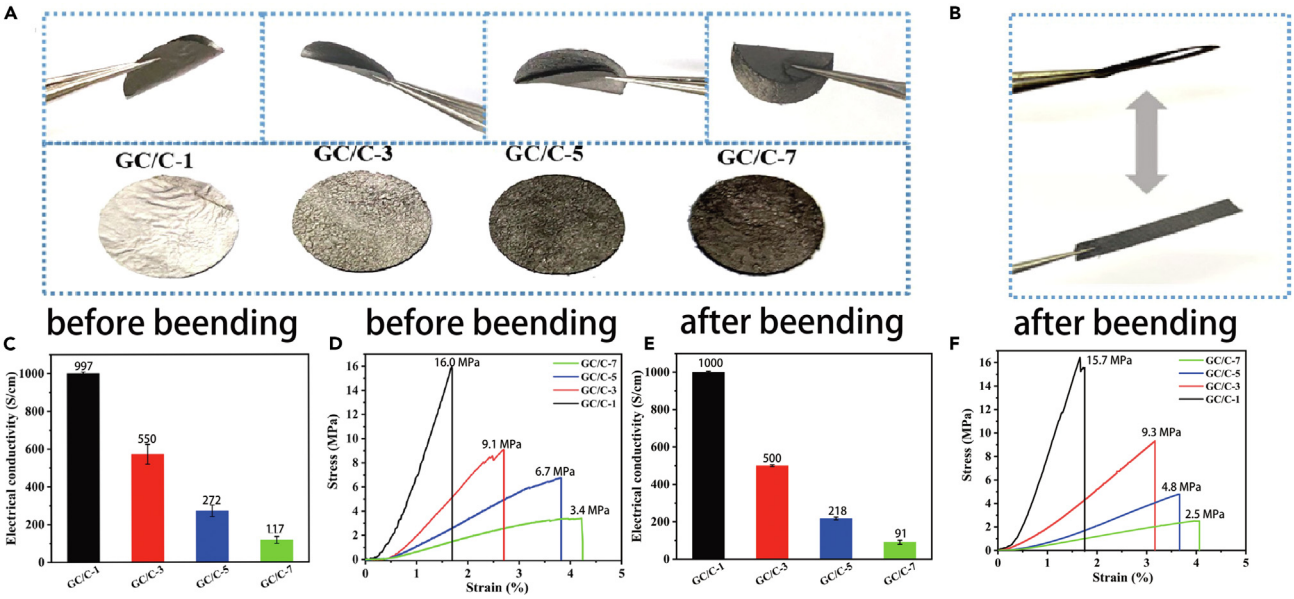

Figure 3. Mechanical properties of GC/C-n films

(A–F) (A) Optical photos of GC/C-n before and after folding; (B) Optical photo of GC/C-7 film after 250 consecutive bending; (C) Conductivity of GC/C-n films before bending; (D) Stress-strain curves of GC/C-n films before continuous bending; (E) Conductivity of GC/C-n film after 250 bending; (F) Stress-strain curves of GC/C-n films after 250 bending.

to GO reduction and formed a good interface between porous carbon and graphene. Nevertheless, half peak width also presents an increasing trend, indicating that the layer spacing is gradually increasing, mainly caused by large number of small gas molecules caused by PVA decomposition, which is well proven in SEM characterization. In the Raman results of the Figure 2I, peak D and peak G appear obviously the same as graphene, and the intensity of peak G is significantly higher than peak D, indicating that graphene has been successfully prepared and presented a lower defect, which is consistent with XRD results.

DISCUSSION

According to the electromagnetic theory, it can be known that the conductivity of materials has a critical impact on its electromagnetic shielding performance in general, since studies have shown that the value of RL increases with the increase of conductivity.[37,38] Therefore, the conductivity of GC/C films was tested first as shown in Figure 3C. The graphene/carbon nanofiber composite film (GC/C-1) prepared by scraping and coating method showed excellent conductivity, which can reach 1000 S/cm. With the increase of the total number of alternating layers, the conductivity of the film shows a gradual decline, which is mainly because the increase of pores in the porous carbon alternating layer leads to the decrease of conductive path, which affects the increase of resistance caused by the free movement of electrons. Nevertheless, the conductivity of GC/C-7 can still reach 117 S/cm, which is significantly higher than most expanded graphene thin films reported in relevant paper.[39,40] Subsequently, the mechanical property was tested in order to explore the possibility of its practical application, which shows a similar trend as conductivity. As shown in Figure 3D, the maximum tensile strength of GC/C-1 can reach 16 MPa, which decreased gradually with the introduction of PVA aerogel, because after high temperature reduction, the gap at the alternating interface of the film would increase, and the contact between the graphene sheets would decrease, thus leading to a decrease in strength. However, due to the strength of graphene and carbon nanofibers themselves and the combination between them, the film still has excellent mechanical properties, which can reach the target required for practical application. In particular, although the strength decreased, the strain showed a trend of gradual increase with the increase of the number of layers. In addition to mechanical strength, flexibility and structural stability are required in order for the film to be effective for long term applications in flexible electronic devices. The films were bent 180° to explore their potential use in flexible devices. The test results show that all GC/C films were able to recover to the initial state after 180° bending and maintain their structural integrity, indicating that the alternating films had good flexibility (Figure 3A). 250 cycles of continuous compression bending test was used to further verify its structural stability (bending radius less than 1 mm) (Figure 3B), electrical conductivity and mechanical properties were tested to verify the stability of its electrical and mechanical properties in Figures 3E and 3F. Compared to GC/C film before cyclic bending, the electrical conductivity and mechanical properties of GC/C film after cyclic bending did not decrease significantly. After stress release, the film can be restored to the initial state, which has good bending property. Specially, with the increase of the number of alternating layers, the proportion of mechanical conductivity decline slightly increases, so the number of alternating layers cannot be too high. The excellent structural stability proves that the alternating film has a good cycle life, and the high conductivity will give the GC/C-n film excellent electromagnetic shielding performance.

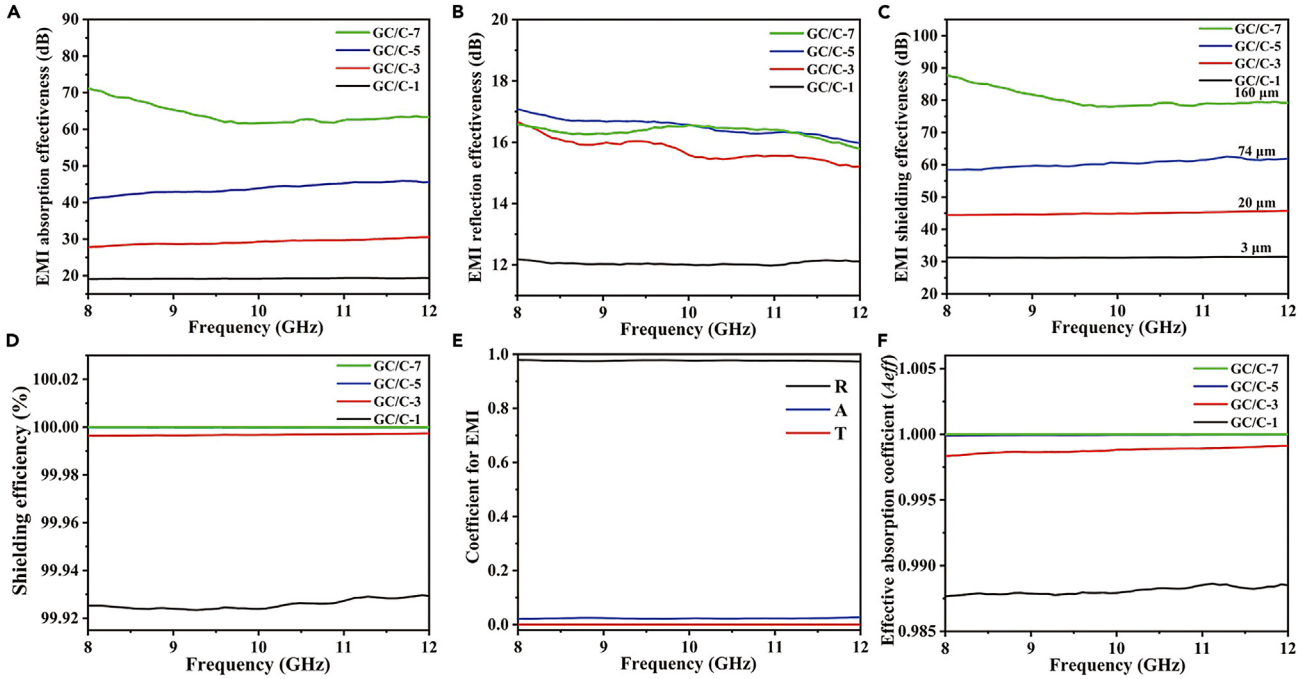

Figure 4. EMI shielding performance testing of GC/C-n films

(A–F) Electromagnetic properties of GC/C-n films at 8.0–12.0 GHz: (A) Total EMI shielding performance (SE_T); (B) EMI absorption effectiveness of GC/C-n films (SE_A); (C) EMI reflection effectiveness of GC/C-n films (SE_R); (D) Shielding efficiency of GC/C-n films; (E) Effective absorption coefficient (Aeff); (F) coefficient for EMI.

Finally, the electromagnetic shielding performance of the film is tested in Figure 4. Comparing with the compact stacked layered graphene film, the microballoon of the graphene and carbon nanofiber composite film prepared in this work and the porous structure of the alternate carbon material have more interfaces, which will promote the multiple reflection loss and absorption of electromagnetic wave, and thus improve the overall shielding performance of the film to a large extent.[35,39–43] As shown in SEM characterization (Figure 2G) that the thickness of the film increases from 3 μm to 160 μm with the increasing of the number of alternating layers, which leads to more interfacial effects and space for multiple reflections of electromagnetic waves. The EMI shielding effectiveness (SE_T) shows excellent performance (Figure 4A) which increases from 32 dB to 80 dB at 8–12 GHz as the amount of alternating layers increases, which is much higher than the commercial requirement of 20 dB. In order to further explore the loss mechanism and better understand the effect of the thin film on electromagnetic waves, the EMI reflection effectiveness (SE_R) and EMI absorption effectiveness (SE_A) are calculated in Figures 4B and 4C, which shows that the value of SE_A (Figure 4B) is higher than SE_R (Figure 4C) obviously, indicating that absorption is the main reason for the excellent EMI shielding effect. A higher SE_A value means that electromagnetic waves entering the interior of the material are attenuated by conduction losses and multiple reflection losses, since the impedance between the air and the graphene sheet does not match, and electromagnetic waves entering the film will be reflected at the corresponding interface. The porous structure of the film allows incoming electromagnetic waves to reflect more internally, resulting in the electromagnetic energy transfer, thus improving the electromagnetic wave absorption. The shielding efficiency is shown in Figure 4D, which range from 99.8700% to 99.99999%, representing that electromagnetic waves are basically expendable by films. The effective absorption coefficient (Aeff) exhibited in Figure 4E indicate that more than 99.9996% of the electromagnetic energy can be suppressed. R, T, and A, the coefficient for EMI has been calculated, the calculation results show that A and T are close to 0 while R is close to 1 (Figure 4F), which means that the electromagnetic energy is almost completely shielded by the film. In particular, as the number of alternating layers of the film increases, the thickness and quality of the film change. Therefore, it is not convincing to consider the influence of the film thickness only on its shielding performance. Based on material density, the effective density (=EMI SE/density) is calculated, and the calculation results are shown in Table 1.

In order to explore the loss mechanism of electromagnetic wave in porous alternating film and prove that the multi-layer alternating structure provides an effective interface for electromagnetic wave attenuation, electromagnetic simulation is carried out through CST software. In this work, it is necessary to explore the structure related to the electromagnetic wave loss mechanism mainly includes porous structure, interface structure, and the structure of alternating changing conductivity. Since porous structure is obviously conducive to electromagnetic wave loss, meanwhile, the conductivity measured in this work is the conductivity of porous structure instead of solid structure, so it is more accurate to choose solid structure model for simulation analysis. Therefore, in order to simplify the establishment of the model and express the electrical conductivity of the materials in the model more accurately, the model was established as a multi-layer alternating structure. The

Table 1. Comparison of EMI shielding properties of films with different alternating layers

	EMI SE (dB)	Thickness (cm)	Mass (g)	Density (g/cm^3)	SSE (dB·cm^3/g)	SSE/t (dB·cm^2/g)
1 layer	31	0.0003	0.0003	0.7538	41.1262	137087.33
3 layer	42	0.002	0.0014	0.5276	79.5990	39799.5
5 layer	59	0.0074	0.0034	0.3463	170.3575	23021.28
7 layer	80	0.016	0.0064	0.3015	265.3300	16583.13

electrical conductivity of the GC layer is set to 100000 S/m which is measured previously, while the the ε of C is set to 15 and the μ is set to 1, which can roughly express the electromagnetic parameters of porous carbon layer. The thickness of conductive layer was set at 0.1 mm, the thickness of porous layer was set at 0.4 mm, and the total thickness of seven thin films was set at 160 μm, which was consistent with the SEM characterization. The size was designed to be 22.86 mm × 10.16 mm, which was consistent with the size of X-band waveguide cavity. The structural model is shown in Figure 5A. The background conditions are set to vacuum, the boundary conditions in the x axis and y axis directions are established as an electric field equal to zero, the electromagnetic wave is along the negative direction of the z axis. The power loss density was calculated first to exhibit the loss ability of different layers film in Figures 5C–5F. As can be seen from the power loss density, the power loss density of single-layer film (Figure 5C) is obviously lower than that of multilayered film (Figures 5D–5F), which proves the importance of multilayer design. In addition, the power loss density of 7-layers film is so large that it can almost shield all electromagnetic waves, which can also be seen from the total electric field distribution (Figure 5B). The 5-layer alternating thin film (Figure 5E) does not achieve such a high loss capacity, which proves that the 7-layer design is necessary. The electric field distribution of the film is then calculated. Then, the electric field intensity was calculated in Figures 5G and 5H, which shows that the electric field intensity on the surface of GC layer is significantly higher than the C layer, which means porous C layer exhibits much lower electric field intensity than the interface, means that the electric field intensity has a sudden change at the interface of the two structures. When the electromagnetic wave incident on the interface, it will be reflected, and the reflection will enter the aerogel pore structure for multiple reflections and absorption, resulting in energy loss,[44,45] which represents that electromagnetic wave will be reflected in multiple stages and brings strong polarization effect, which is beneficial to electromagnetic wave loss.

The mechanism of GC/C-n for excellent EMI shielding is schematically illustrated in Figure 6. Due to the high surface conductivity of graphene and carbon nanofibers in the GC layer, partial electromagnetic wave will be reflected directly, which can be explained by impedance mismatch. Electromagnetic waves entering GC/C-n films are first partially consumed by the synergistic conduction loss of graphene and carbon nanofibers, then the electromagnetic wave entering the alternating interface is attenuated at the interface by polarization loss and multiple reflections at the porous carbon.[46~48] According to the results of finite element analysis, there are multiple internal reflections of electromagnetic waves in the multi-layer alternating structure, which will also benefit the loss of electromagnetic waves. Compared with the dense carbon film without structural design, the film prepared in this work has better shielding performance. Therefore, the structural design plays a key role in this work, because the multiple reflection and scattering of electromagnetic waves caused by the structure becomes the dominant factor for the excellent shielding performance. Besides, the continuous conductive network constructed by carbon nanofibers is also an essential reason for the effective transmission and attenuation of electromagnetic wave. The aforementioned reasons are effective to the film to achieve high shielding performance.

In this paper, by referring to the multistage interface and layered structure of multi-layer steamed bread, GO/aPAN nanofibers were used as solution and PVA aerogel film was used as the base to prepare composite alternating film by scraping and coating. Then, the multilayer porous alternating graphene based film was prepared by high-temperature annealing reduction. The multi-layer alternating structure constructed by PVA and GO/aPAN nanofibers after annealing at high temperature will further increase the multiple reflection absorption of electromagnetic wave, polarization at the interface and conductive loss of both will be conducive to its wide application in the field of EMI shielding. In the range of 8–12 GHz, the EMI shielding value increases from 32 dB to 80 dB, and the shielding efficiency increases from 99.87000% to 99.99999%. The relevant parameters of other working electromagnetic shielding films are listed in the supporting information section (Table S1), which has good shielding properties or mechanical properties. However, the feature of this paper is that the number of layers can be controlled, and the mechanical properties and electromagnetic shielding properties can be improved uniformly. In particular, the film can reach 80 dB EMI when the tensile strength is sufficient to support the film, so light thin films with appropriate tensile strength and EMI shielding properties can be selected according to the actual application situation through the regulation of the number of layers, providing the prospect of long-term effective application in flexible equipment and an idea for novel structure design of graphene-based thin films.

STAR★METHODS

Detailed methods are provided in the online version of this paper and include the following:

- KEY RESOURCES TABLE
- RESOURCE AVAILABILITY
  - Lead contact

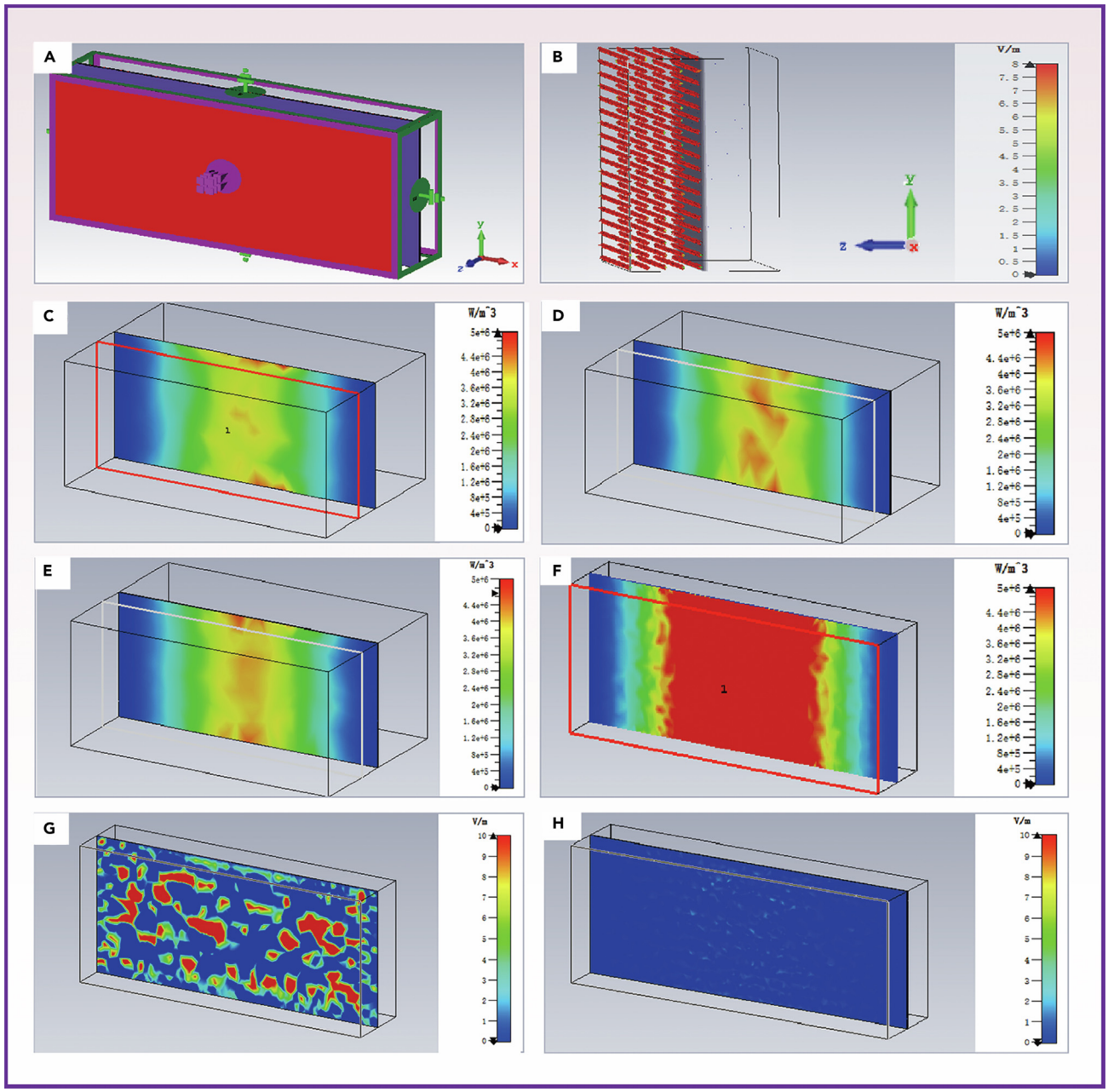

Figure 5. Electromagnetic simulation of GC/C-n films

(A–H) CST simulation results of multilayered structure at 8–12 GHz: (A) Electromagnetic shielding simulation model of multilayered structure; (B–F) Electric field intensity distribution of (B) vector component of seven layers film; (c) one layer film; (D) three layers film; (E) five layers film; (F) seven layers film; (G and H) Power loss density of (G) GC layer; (H) C layer.

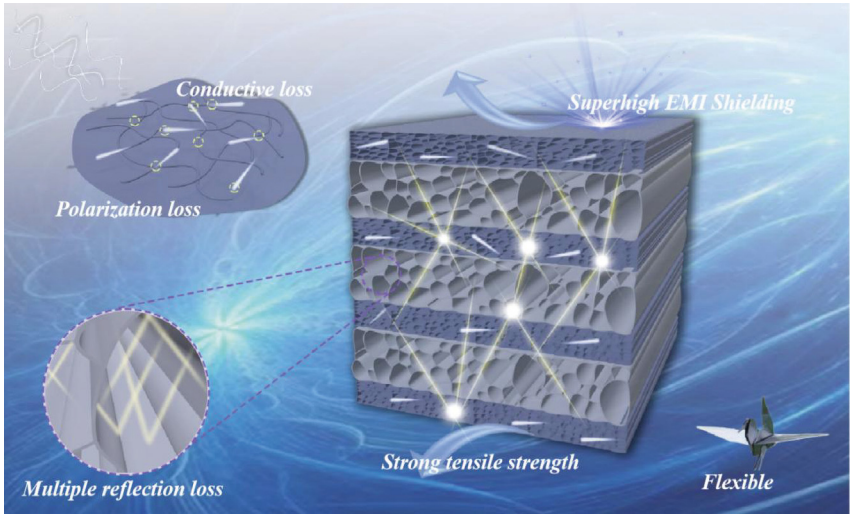

Figure 6. EMI shielding mechanism of the GC/C-7 film

- Electromagnetic simulation of alternating multilayered film
- QUANTIFICATION AND STATISTICAL ANALYSIS
- ADDITIONAL RESOURCES

SUPPLEMENTAL INFORMATION

Supplemental information can be found online at https://doi.org/10.1016/j.isci.2023.107975.

ACKNOWLEDGMENTS

This work was financially supported by the National Natural Science Foundation of China (NSFC, Nos. 51903213, 5217130190, and 52172081), the Science and Technology Planning Project of Sichuan Province (Nos. 2023NSFSC1952 and 2022ZYD0028), the Central Government Guides the Local Science and Technology Development Special Funds (No. 2021Szvup124), and the Fundamental Research Funds for the Central Universities (No. 2682021GF004) to freely explore basic research projects. In addition, the authors would like to thank the Analytical and Testing Center of Southwest Jiaotong University for supporting the relative measurements. They are also grateful for the VCD analysis provided by Shanghai Research Dog Technology Co. Ltd.

AUTHOR CONTRIBUTIONS

J.T.L.: Data curation, Formal analysis, Visualization, Software, Writing – original draft, Validation, Writing – review & editing. J.Z.L.: Conceptualization, Methodology, Investigation, Data curation, Formal analysis, Visualization, Software. T.L.: Methodology, Investigation, Data curation, Formal analysis. Z.X.: Data curation, Formal analysis, Y.C.: Methodology, Validation, Writing – review & editing. L.Z.: Methodology, Validation, Writing – review & editing. Q.Q.: Review, editing and investigation. B.L.: Investigation, Data curation, Supervision, Funding acquisition. F.M.: Investigation, Data curation, Supervision, Funding acquisition, Project administration.

DECLARATION OF INTERESTS

The authors declare no competing interests.

INCLUSION AND DIVERSITY

We support inclusive, diverse, and equitable conduct of research.

Received: May 25, 2023
Revised: July 17, 2023
Accepted: September 15, 2023
Published: September 21, 2023

REFERENCES

1. Zhang, X.J., Wang, G.S., Cao, W.Q., Wei, Y.Z., Liang, J.F., Guo, L., and Cao, M.S. (2014). Enhanced Microwave Absorption Property of Reduced Graphene Oxide (RGO)-MnFe2O4 Nanocomposites and Polyvinylidene Fluoride. ACS Appl. Mater. Interfaces *6*, 7471–7478. https://doi.org/10.1021/am500862g.
2. Liu, P., Gao, S., Zhang, G., Huang, Y., You, W., and Che, R. (2021). Hollow Engineering to Co@N-Doped Carbon Nanocages via Synergistic Protecting-Etching Strategy for Ultrahigh Microwave Absorption. Adv. Funct. Mater. *31*, 2102812. https://doi.org/10.1002/adfm.202102812.
3. Xu, Z., Li, J., Li, J., Du, J., Li, T., Zeng, W., Qiu, J., and Meng, F. (2023). Bionic structures for optimizing the design of stealth materials. Phys. Chem. Chem. Phys. *25*, 5913–5925. https://doi.org/10.1039/d2cp06086h.
4. Chen, Y., Li, J., Li, T., Zhang, L., and Meng, F. (2021). Recent advances in graphene-based films for electromagnetic interference shielding: Review and future prospects. Carbon *180*, 163–184. https://doi.org/10.1016/j.carbon.2021.04.091.
5. Peng, H.K., Wang, Y., Li, T.T., Lou, C.W., He, Q., and Lin, J.H. (2019). Superhydrophobic/Flame Retardant/EMI Shielding Fabrics: Manufacturing Techniques and Property Evaluations. Appl. Sci. *9*, 1914. https://doi.org/10.3390/app9091914.
6. Jia, Z., Lan, D., Lin, K., Qin, M., Kou, K., Wu, G., and Wu, H. (2018). Progress in low-frequency microwave absorbing materials. J. Mater. Sci. Mater. Electron. *29*, 17122–17136. https://doi.org/10.1007/s10854-018-9909-z.
7. Liu, L., Deng, H., Tang, X., Lu, Y., Zhou, J., Wang, X., Zhao, Y., Huang, B., and Shi, Y. (2021). Specific electromagnetic radiation in the wireless signal range increases wakefulness in mice. Proc. Natl. Acad. Sci. USA *118*. https://doi.org/10.1073/pnas.2105838118cx.
8. Zhao, T., Jia, Z., Zhang, Y., and Wu, G. (2023). Multiphase Molybdenum Carbide Doped Carbon Hollow Sphere Engineering: The Superiority of Unique Double-Shell Structure in Microwave Absorption. Small *19*, 2206323. https://doi.org/10.1002/smll.202206323.
9. Li, T., Li, J., Xu, Z., Tian, Y., Li, J., Du, J., and Meng, F. (2023). Electromagnetic Response of Multistage-Helical Nano-Micro Conducting Polymer Structures and their Enhanced Attenuation Mechanism of Multiscale-Chiral Synergistic Effect. Small *19*, 2300233. https://doi.org/10.1002/smll.202300233.
10. Li, W., Shang, L., Huang, K., Li, J., Wang, Z., and Yao, H. (2017). Flexible and easy-to-tune broadband electromagnetic wave absorber based on carbon resistive film sandwiched by silicon rubber/multi-walled carbon nanotube composites. Carbon *8*, 544–549. https://doi.org/10.1016/j.carbon.2017.06.034.
11. Wang, Y.L., Wang, G.S., Zhang, X.J., and Gao, C. (2022). Porous carbon polyhedrons coupled with bimetallic CoNi alloys for frequency selective wave absorption at ultralow filler loading. J. Mater. Sci. Technol. *103*, 34–41. https://doi.org/10.1016/j.jmst.2021.06.021.
12. Gong, S., Sheng, M., Li, X., Sheng, X., Wu, H., Lu, X., and Qu, J. (2022). A Multifunctional Flexible Composite Film with Excellent Multi-Source Driven Thermal Management, Electromagnetic Interference Shielding, and Fire Safety Performance, Inspired by a "Brick–Mortar" Sandwich Structure. Adv. Funct. Mater. *32*, 2200570. https://doi.org/10.1002/adfm.202200570.
13. Zhang, S., Peng, Y., Fan, H., Zhang, Y., and Min, P. (2022). Multifunctional Ti3C2Tx-(Fe3O4/polyimide) composite films with Janus structure for outstanding electromagnetic interference shielding and superior visual thermal management. Nano Res. *21*, 5601–5609. https://doi.org/10.1007/s12274-022-4358-7.
14. Jiang, X., Zhou, J., Zhong, X., Hu, Z., Hu, R., Song, Y., and Zheng, Q. (2023). Stretchable PEDOT:PSS/Li-TFSI/XSB Composite Films for Electromagnetic Interference Shielding. ACS Appl. Mater. Interfaces *15*, 8521–8529. https://doi.org/10.1021/acsami.2c21604.
15. Li, L., Zhao, S., Luo, X.J., Zhang, H.B., and Yu, Z.Z. (2021). Smart MXene-Based Janus films with multi-responsive actuation capability and high electromagnetic interference shielding performances. Carbon *175*, 594–602. https://doi.org/10.1016/j.carbon.2020.10.090.
16. Zhang, L., Chen, Y., Liu, Q., Deng, W., Yue, Y., and Meng, F. (2022). Ultrathin flexible electrospun carbon nanofibers reinforced graphene microgasbags films with three-dimensional conductive network toward synergetic enhanced electromagnetic interference shielding. J. Mater. Sci. Technol. *111*, 57–65. https://doi.org/10.1016/j.jmst.2021.08.090.
17. Zhao, Z., Zhang, B., Du, Y., Hei, Y., Yi, X., Shi, F., and Xian, G. (2017). MWCNT modified structure-conductive composite and its electromagnetic shielding behavior. Compos. Part B *130*, 21–27. https://doi.org/10.1016/j.compositesb.2017.07.033.
18. Guan, Q.F., Han, Z.M., Yang, K.P., Yang, H.B., Ling, Z.C., Yin, C.H., and Yu, S.H. (2021). Sustainable Double-Network Structural Materials for Electromagnetic Shielding. Nano Lett. *21*, 2532–2537. https://doi.org/10.1021/acs.nanolett.0c05081.
19. Ye, J., Chen, X., Luo, Z., Li, J., Yuan, Y., Tan, J., and Pan, F. (2021). Improving Strength and Electromagnetic Shielding Effectiveness of Mg–Sn–Zn–Ca–Ce Alloy by Sn Addition. Adv. Eng. Mater. *23*. https://doi.org/10.1002/adem.202100166.
20. Novoselov, K.S., Geim, A.K., Morozov, S.V., Jiang, D., Zhang, Y., Dubonos, S.V., Grigorieva, I.V., and Firsov, A.A. (2004). Electric Field Effect in Atomically Thin Carbon Films. Science *306*, 666–669.
21. Geim, A.K. (2009). Graphene: status and prospects. Science *324*, 1530–1534.
22. Sun, X., He, J., Li, G., Tang, J., Wang, T., Guo, Y., and Xue, H. (2013). Laminated magnetic graphene with enhanced electromagnetic wave absorption properties. J. Mater. Chem. C *1*, 765–777. https://doi.org/10.1039/c2tc00159d.
23. Yang, Q., Yang, J., Tang, L., Zhang, H., Wei, D., Shi, H., Wei, X., Zhang, Y., and Su, B. (2023). Superhydrophobic graphene nanowalls for electromagnetic interference shielding and infrared photodetection via a two-step transfer method. Chem. Eng. J. *454*, 140159. https://doi.org/10.1016/j.cej.2022.140159.
24. Pei, X., Liu, G., Shi, H., Yu, .R., Wang, S., Liu, S., Min, C., Song, J., Shao, R., and Xu, Z. (2023). Directional electromagnetic interference shielding of asymmetric structure based on dual-needle 3D printing. Compos. Sci. Technol. *233*, 109909. https://doi.org/10.1016/j.compscitech.2023.109909.
25. Meng, F., Chen, Y., Liu, W., Zhang, L., Deng, W., and Zhao, Z. (2022). Multifunctional RGO-based films with "brick-slurry" structure: High-efficiency electromagnetic shielding performance, high strength and excellent environmental adaptability. Carbon *200*, 156–165. https://doi.org/10.1016/j.carbon.2022.07.052.
26. Zhang, Y., Ruan, K., Shi, X., Qiu, H., Pan, Y., Yan, Y., and Gu, J. (2021). Ti3C2Tx/rGO porous composite films with superior electromagnetic interference shielding performances. Carbon *175*, 271–280. https://doi.org/10.1016/j.carbon.2020.12.084.
27. Liang, L., Xu, P., Wang, Y., Shang, Y., Ma, J., Su, F., Feng, Y., He, C., Wang, Y., and Liu, C. (2020). Flexible polyvinylidene fluoride film with alternating oriented graphene/Ni nanochains for electromagnetic interference shielding and thermal management. Chem. Eng. J. *395*, 125209. https://doi.org/10.1016/j.cej.2020.125209.
28. Wang, Y.L., Yang, S.H., Wang, H.Y., Wang, G.S., Sun, X.B., and Yin, P.G. (2020). Hollow porous CoNi/C composite nanomaterials derived from MOFs for efficient and lightweight electromagnetic wave absorber. Carbon *167*, 485–494. https://doi.org/10.1016/j.carbon.2020.06.014.
29. Zhang, Y., Xu, M.K., Wang, Z., Zhao, T., Liu, L.X., Zhang, H.B., and Yu, Z.Z. (2022). Strong and conductive reduced graphene oxide-MXene porous films for efficient electromagnetic interference shielding. Nano Res. *15*, 4916–4924. https://doi.org/10.1007/s12274-022-4311-9.
30. Wang, M., Tang, X.-H., Cai, J.-H., Wu, H., Shen, J.-B., and Guo, S.-Y. (2021). Construction, mechanism and prospective of conductive polymer composites with multiple interfaces for electromagnetic interference shielding: A review. Carbon *177*, 377–402. https://doi.org/10.1016/j.carbon.2021.02.047.
31. Zhou, B., Zhang, Z., Li, Y., Han, G., Feng, Y., Wang, B., Zhang, D., Ma, J., and Liu, C. (2020). Flexible, Robust, and Multifunctional Electromagnetic Interference Shielding Film with Alternating Cellulose Nanofiber and MXene Layers. ACS Appl. Mater. Interfaces *12*, 4895–4905. https://doi.org/10.1021/acsami.9b19768.
32. Paliotta, L., De Bellis, G., Tamburrano, A., Marra, F., Rinaldi, A., Balijepalli, S.K., Kaciulis, S., and Sarto, M.S. (2015). Highly conductive multilayer-graphene paper as a flexible lightweight electromagnetic shield. Carbon *89*, 260–271. https://doi.org/10.1016/j.carbon.2015.03.043.
33. Hu, G., Wu, C., Wang, Q., Dong, F., and Xiong, Y. (2022). Ultrathin nanocomposite films with asymmetric gradient alternating multilayer structures exhibit excellent electromagnetic interference shielding performances and robust mechanical properties. Chem. Eng. J. *447*, 137537. https://doi.org/10.1016/j.cej.2022.137537.

34. Schulz, R.B., Plantz, V.C., and Brush, D.R. (1988). Shielding theory and practice. IEEE Trans. Electromagn C. *30*, 187–201.
35. Shi, Y., Xiang, Z., Cai, L., Pan, F., Dong, Y., Zhu, X., Cheng, J., Jiang, H., and Lu, W. (2022). Multi-interface Assembled N-Doped MXene/HCFG/AgNW Films for Wearable Electromagnetic Shielding Devices with Multimodal Energy Conversion and Healthcare Monitoring Performances. ACS Nano *16*, 7816–7833. https://doi.org/10.1021/acsnano.2c00448.
36. Guo, T., Li, C., Wang, Y., Wang, Y., Yue, J., and Tang, X.Z. (2020). A highly flexible and porous graphene-based hybrid film with superior mechanical strength for effective electromagnetic interference shielding. Appl. Phys. *126*, 776. https://doi.org/10.1007/s00339-020-03965-w.
37. Tian, K., Hu, D., Wei, Q., Fu, Q., and Deng, H. (2023). Recent progress on multifunctional electromagnetic interference shielding polymer composites. J. Mater. Sci. Technol. *134*, 106–131. https://doi.org/10.1016/j.jmst.2022.06.031.
38. Orasugh, J.T., and Ray, S.S. (2023). Functional and Structural Facts of Effective Electromagnetic Interference Shielding Materials: A Review. ACS Omega *8*, 8134–8158. https://doi.org/10.1021/acsomega.2c05815.
39. Wang, X.Y., Liao, S.Y., Huang, H.P., Hu, Y.G., Zhu, P.L., Sun, R., and Wan, Y.J. (2022). Graphene Oxide/Carbon Tube Composite Films with Tunable Porous Structures for Electromagnetic Interference Shielding. ACS Appl. Nano Mater. *5*, 13509–13518. https://doi.org/10.1021/acsanm.2c03071.
40. Tian, J., Yang, J., Yang, C., and Hao, S. (2019). Compression and reduction of graphene oxide aerogels into flexible, porous and functional graphene films. J. Mater. Sci. *54*, 13147–13156. https://doi.org/10.1007/s10853-019-03828-7.
41. Zhang, Y., Zhang, G., Shi, X., Gao, Q., Huang, F., and Xiao, R. (2021). A flexible and strong reduced graphene oxide film for high-performance electromagnetic shielding. Compos. Commun. *28*, 100954. https://doi.org/10.1016/j.coco.2021.100954.
42. Liu, P., Zhang, G., Xu, H., Cheng, S., Huang, Y., Ouyang, B., Qian, Y., Zhang, R., and Che, R. (2023). Synergistic Dielectric–Magnetic Enhancement via Phase-Evolution Engineering and Dynamic Magnetic Resonance. Adv. Funct. Mater. *33*, 2211298. https://doi.org/10.1002/adfm.202211298.
43. Liu, P., Wang, Y., Zhang, G., Huang, Y., Zhang, R., Liu, X., Zhang, X., and Che, R. (2022). Hierarchical Engineering of Double-Shelled Nanotubes toward Hetero-Interfaces Induced Polarization and Microscale Magnetic Interaction. Adv. Funct. Mater. *32*, 2202558. https://doi.org/10.1002/adfm.202202588.
44. Cai, Z., Su, L., Wang, H., Niu, M., Tao, L., Lu, D., Xu, L., Li, M., and Gao, H. (2021). Alternating Multilayered Si3N4/SiC Aerogels for Broadband and High-Temperature Electromagnetic Wave Absorption up to 1000 °C. ACS Appl. Mater. Interfaces *13*, 16704–16712. https://doi.org/10.1021/acsami.1c02906.
45. Chen, J., Wang, Y., Liu, Y., Tan, Y., Zhang, J., Liu, P., and Kong, J. (2023). Fabrication of macroporous magnetic carbon fibers via the cooperative etching-electrospinning technology toward ultra-light microwave absorption. Carbon *208*, 82–91. https://doi.org/10.1016/j.carbon.2023.03.043.
46. Shi, B., Liang, H., Xie, Z., Chang, Q., and Wu, H. (2023). Dielectric loss enhancement induced by the microstructure of CoFe2O4 foam to realize broadband electromagnetic wave absorption. Int. J. Miner. Metall. Mater. *30*, 1388–1397. https://doi.org/10.1007/s12613-023-2599-4.
47. Chang, Q., Liang, H., Shi, B., and Wu, H. (2022). Microstructure induced dielectric loss in lightweight Fe3O4 foam for electromagnetic wave absorption. iScience *25*, 103925. https://doi.org/10.1016/j.isci.2022.103925.
48. Wang, H.Y., Sun, X.B., Xin, Y., Yang, S.H., Hu, P.F., and Wang, G.S. (2023). Ultrathin self-assembly MXene/Co-based bimetallic oxide heterostructures as superior and modulated microwave absorber. J. Mater. Sci. Technol. *134*, 132–141. https://doi.org/10.1016/j.jmst.2022.05.061.

STAR★METHODS

KEY RESOURCES TABLE

REAGENT or RESOURCE	SOURCE	IDENTIFIER
Chemicals, peptides, and recombinant proteins		
Polyacrylonitrile powder	Kelong	Mw=150000
N,N-dimethylformamide	Sigma-Aldrich Chemical	CAS-68-12-2
Aqueous GO solution	Hangzhou Gaoxi Technology	10 mg/g
Polyvinyl alcohol 1788	Chengdu Haihong Experimental Instrument	CAS-9002-89-5

RESOURCE AVAILABILITY

Lead contact

Further information and requests for resources and reagents should be directed to and will be fulfilled by the lead contact, Fanbin Meng. (mengfanbin_wing@126.com).

Materials availability

This work did not generate new unique reagents.

Data and code availability

Any additional information required to reanalyze the data reported in this paper is available from the lead contact upon reasonable request.

METHOD DETAILS

Materials

Polyacrylonitrile powder (PAN, Mw=150000) was purchased from Kelong Chemical Co. (Chengdu, China). The alkali-treated polyacrylonitrile (aPAN) was prepared by N,N-dimethylformamide (DMF) and Sodium hydroxide (NaOH) (Sigma-Aldrich Chemical Co.) Aqueous GO solution (10.0 mg/mL) was purchased from Hangzhou Gaoxi Technology Co. Ltd. Polyvinyl alcohol 1788 (PVA) was purchased from Chengdu Haihong Experimental Instrument Co. Ltd. All reagents were used without further purification.

Preparation of GC/C-n alternating reduction film

Preparation of PVA aerogel film

5 g PVA powder was dissolved in 95 mL deionized water with stirring for 4 hours at 60°C. The solution was added to smooth petri dishes after cooled to room temperature, then it was frozen with liquid nitrogen and freeze-dried for 48 hours. Multiple samples were prepared for later use.

Preparation of GO/aPAN solution

Initially, 10 g PAN powder was dissolved in 90 g DMF with stirring at 60°C for 3 hours to obtain 10 wt% PAN solution. PAN nanofibers film was manufactured by electrospinning (20 G stainless steel needle, 2 μL/min velocity of flow, voltage of 15 kV, collecting plate of 15 cm). The electrospun fibers film was dried in a vacuum oven at 60°C for 24 hours. Then the electrospun fibers film was alkaline treated by immersing into 1 M NaOH aqueous solution at 40°C for 2 h according to the reference[16]. Then it was dispersed at 10000-12000 rpm by a high-speed homogenous disperser after washing with deionized water (DW), and finally dried in oven at 60°C overnight. Afterwards, the aPAN nanofibers were manufactured.

Subsequently, 10 mg aPAN was dissolved in 2.5 mL DW with ultrasonic dispersion to get uniform aPAN nanofiber solution, which was mixed with 10 g GO solution (10 mg/g) and stirred to get uniform GO-aPAN solution.

Preparation of GO/aPAN-PVA-n alternate film

A layer of PVA aerogel film was placed on the flat substrate, and then the Go-aPAN solution was scraped and coated by a scaler (Tianjin Kexin Test Airport KTQ-II) on the other side of the PVA film after air drying ,coating thickness is set to 3 mm, then the multi-layer alternating film was prepared according to the above method, which was named as GO/aPAN-PVA-n film (n is the total number of layers of the film).

Preparation of GC/C-n alternating reduction film

Firstly, GO/aPAN-PVA-n film was preoxidized in muffle furnace by heating to 200°C and helding for 40 min. Subsequently, the pre-oxidized film was then carbonized in a graphite furnace and heated to 1200°C (10°C/min rate of heating) and again to 1900°C (5°C/min rate of heating) for 1.5 h. After the procedure, the carbonized film was naturally cooled to room temperature. The whole process was carried out in vacuum. Finally, graphene-carbon nanofiber/carbon aerogel was prepared and named GC/C-n (n is the total number of layers of the film).

Characterization of GO/aPAN-PVA-n and GC/C-n film

The morphology and the fracture surface of the different composite papers were investigated by field-emission scanning electron microscopy (FESEM, QANPA200, FEI). The structure of the composite films was analyzed by using an X-ray diffraction system (XRD, PW1830, Philips) with a Cu-Kα radiation from 5 to 60°. The Raman spectrum (In Via, Renshaw) excited by a 532 nm laser was tested in the wavenumber range of 1000-3000 cm^{-1}. The electrical conductivity of the samples was measured using a standard fourprobe method on a 4-Point Probes Resistivity Measurement System. Stress-strain curves were measured by a small testing machine (XS (08) XT03, Xu Sai) with a loading rate of 0.1 mm/min at room temperature (at least six samples).

EMI shielding effectiveness measurement

EMI shielding effectiveness measurements were carried out using an Agilent PNA E501C vector network analyzer in the frequency range between 8 and 12 GHz. The S parameters (S11, S21, S22, and S12) derived from the vector network analyzer can be used to calculate the absorption coefficient (A), reflection coefficient (R), transmission coefficient (T), SE absorption (SEA), SE reflection (SER) and SE total (SET):[34]

$$T = |s_{11}|^2 = |s_{22}|^2$$

$$R = |s_{12}|^2 = |s_{21}|^2$$

$$A = 1 - T - R$$

$$SE_R = -10\,log_{10}(1 - R)$$

$$SE_A = -10\,log_{10}[T/(1 - R)]$$

$$SE_T = SE_A + SE_R$$

Electromagnetic simulation of alternating multilayered film

The CST electromagnetic simulation software (CST Studio Suite 2021) was used for modeling to analyze the loss mechanism of the alternating multilayer film. The simulation was conducted by frequency domain simulator and the whole structure was simulated under ideal boundary conditions where the electric field was zero. Since it is obvious that the porous structure is conducive to the internal multiple reflection of electromagnetic wave, the simulation only needs to explore the effect of multilevel structure, especially the alternating structure on internal electromagnetic wave. Therefore, in order to simplify the establishment of the model and reduce the complexity of calculation, the film was only established into a multilayer alternating structure model in order to explore the electromagnetic wave loss mechanism inside. Frequency in the whole simulation ranged from 8 to 12 GHz.

QUANTIFICATION AND STATISTICAL ANALYSIS

All mean values are expressed in the form of error bars.

ADDITIONAL RESOURCES

This work did not contain additional resources.